47th AIAA Aerospace Sciences Meeting Including The New Horizons Forum and Aerospace Exposition
5 - 8 January 2009, Orlando, Florida
AIAA 2009-585

DNS Study of Transient Disturbance Growth and Bypass Transition Due to Realistic Roughness

Kelly A. Stephani‡ and David B. Goldstein†
The University of Texas at Austin, Austin, TX 78712-0235

Direct numerical simulation was used to investigate the detailed flow past a periodic array of cylindrical roughness elements. A spectral DNS code was used to model flow over a flat plate surface, and roughness elements were formed using an immersed boundary technique. Solutions were obtained for two roughness heights corresponding to Reynolds numbers (Re_k) of 202 and 334, and results are presented for both cases. Cylindrical roughness elements with Re_k=202 produced minimal disturbances and the flow appeared generally laminar in the wake downstream of the roughness elements. Flow past cylindrical roughness elements corresponding to Re_k=334 was found to transition as soon as 2-3 cylinder diameters downstream and had developed into fully turbulent flow by the end of the domain. Results were found to compare reasonably well with a similar set of DNS computations by Rizzetta and Visbal[1] using a sixth-order-accurate centered compact finite difference scheme as well as experimental results obtained by Ergin and White[2] using time-averaged hotwire measurements of the velocity components.

Nomenclature

d	cylindrical roughness diameter, 6.35mm
k	cylindrical roughness height
Re_k	roughness-based Reynolds number ($u(k)k/\upsilon$)
Re_d	diameter-based Reynolds number ($U_\infty d/\upsilon$)
Re_c	code Reynolds number (ν^{-1})
ν	reference kinematic viscosity, $1.5\text{x}10^{-5}$ m^2s^{-1}
U_∞	reference freestream flow speed, 12.2 m s^{-1}
η	non-dimensional wall-normal distance (y/δ)
λ	spacing between roughness elements, 19 mm
$\vec{F}(\vec{x}_s, t)$	immersed boundary force applied at prescribed location/time in domain
α, β	gain constants used in calculation of immersed boundary force field
ΔU	velocity increment used in calculation of immersed boundary force field
$\vec{U}, \vec{U}_{des}$	actual and desired velocity at a particular location in computational domain
x, y, z	Cartesian coordinates in streamwise, vertical and spanwise directions
u, v, w	instantaneous velocity components in x, y and z directions
$\bar{u}, \bar{v}, \bar{w}$	time-averaged velocity components in x, y and z directions
u', v', w'	fluctuating (root-mean-square) velocity components in x, y and z directions
$\omega_x, \omega_y, \omega_z$	instantaneous vorticity components in x, y and z directions
$\lvert\omega\rvert$	magnitude of total vorticity, $\sqrt{\omega_x^2 + \omega_y^2 + \omega_z^2}$
X_L, Y_L, Z_L	length of computational domain in x, y and z directions
N_X, N_Y, N_Z	number of grid points in x, y and z directions

‡ Graduate Research Assistant, Aerospace Engineering Department, Student Member AIAA.
†Professor, Aerospace Engineering Department, Senior Member AIAA.

I. Introduction

Early studies of laminar-turbulent transition were focused primarily on linear stability theory analysis in conjunction with experimental observations. While linear stability analysis provides an analytic approach for determining the disturbances to which a boundary layer is unstable and how a particular instability grows, the formulation of the stability equations is founded upon the assumption of a *small* disturbance, and the analysis may only be used to predict the exponential growth of these disturbances. A difficulty in predicting transition arises due to the issue that in practice, disturbances that cause transition subcritical with respect to the T-S neutral curve may originate from substantial perturbations in the freestream flow or distributed surface roughness. These finite disturbances are thought to lead to transient disturbance growth or even trigger turbulence directly, hence bypassing the primary T-S instability mechanism which is a transition process coined by Morkovin[3] as bypass transition.

Although a complete nonlinear transition theory does not yet exist for analysis of this bypass mechanism, recent literature suggests that transient growth may be one suitable mechanism describing the bypass transition process. The transient growth mechanism was described early on by Landahl's[4] "lift-up" mechanism. It was thought that decaying streamwise vortices near the wall generated by the roughness worked to transport high-velocity flow into low-velocity regions and vice-versa, creating streamwise streaks of high- and low-speed flow observed experimentally in transitional and turbulent flow. Schmid and Henningson[5] present the transient growth mechanism in terms of the Orr-Sommerfeld and Squire eigenfunctions, which are obtained from linear stability analysis. Briefly, it is shown that due to the non-orthogonal nature of the T-S and Squire modes, the superposition of the two decaying exponential modes produces a transient mode which grows algebraically followed by exponential decay. The transient growth processes occur subcritical to the T-S neutral curve, and may be a significant factor in the transition of flows that are otherwise stable to T-S modes[9]. Numerical experiments by Andersson *et al.*[7] investigating maximum spatial transient growth for steady disturbances in the Blasius boundary layer conclude that the largest energy growth in the streamwise streaks is triggered by streamwise vortices. Experiments by Reshotko and Leventhal[8] showed similar transient growth phenomena. This group examined the response of flat plate boundary layer flow to finite perturbations introduced via distributed roughness of Re_k=155 on the surface of the plate near the leading edge. In all cases observed, the onset of instabilities occurred subcritical to the T-S neutral curve, with stronger growth occurring for the lower frequency disturbances.

Ongoing experimental investigations initiated at Case Western Reserve University by Ergin and White[2] and continuing at Texas A&M University by Downs, White and Dennisen[9] have used various distributed roughness geometries on a flat plate surface to study the effect of roughness-induced transient disturbances on boundary layer transition. Hotwire probes were used to acquire streamwise velocity measurements in the wake downstream of the roughness element for various values of Re_k. The cases that were investigated involved roughness elements with corresponding Re_k values that lead to either fully laminar wakes or produce fully turbulent flow downstream of the roughness. The evolution of the flow was analyzed by tracking the magnitude of the unsteady velocity fluctuations and the total disturbance energy at various downstream locations. The discrete cylindrical roughness elements used in the earlier study by Ergin and White exhibited rapid growth of the unsteady velocity fluctuations for the Re_k=334 case, and the power spectra indicated a fully turbulent flow 0.175m downstream of the roughness, with the boundary layer flow being most unstable to the 700Hz disturbance. The unsteady disturbance energy exhibits exponential growth prior to transition for the Re_k=334 case, while the other cases analyzed (Re_k=202 and 264) show only a small streamwise increase in the unsteady disturbance energy. The authors suggest that the fluctuations observed in these cases are likely to be a Kelvin-Helmholtz instability rather than unsteady transient disturbances.

Recent numerical experiments by Rizzetta and Visbal used direct numerical simulation to examine the detailed flow about distributed cylindrical roughness elements on a flat plate[1]. The computational domain was modeled using a sixth-order-accurate centered compact finite-difference scheme to approximate spatial derivatives, and an implicit time marching algorithm with Newton-like subiterations for second-order accuracy in time. The roughness elements examined in their paper had a diameter of 6.35 mm and roughness heights corresponding to Re_k=202 and Re_k=334. Both flow cases were characterized by a pair of counter-rotating horseshoe vortices originating just upstream of the roughness. The flow downstream of the roughness element in the Re_k=202 case exhibited only low-amplitude fluctuations and the wake remained laminar throughout the rest of the domain. The Re_k=334 case exhibited transition almost immediately downstream of the roughness element.

A greater knowledge of transitional and turbulent boundary layer flows, including their formation, growth and detailed flow structures, is essential to numerous applications in aerodynamics. Experimental studies of transitional flows are critical, particularly for cases involving high Reynolds number flows or detailed analysis over wide ranges of spatial and temporal scales which may become quite costly to simulate. However, limitations of experimental instrumentation used in acquiring flow field data make it challenging to provide a complete description of the interactions of the near-surface flow field structures with the surface itself and with the freestream. A joint study underway at UT and Texas A&M University of transitional flow using both experiments and direct numerical simulations (DNS) of the Navier Stokes equations provides a more complete picture of the transition process and may help to elucidate the formation process and interaction of the flow structures which lead to transient disturbance growth and bypass transition. The aim of this paper is to validate the results obtained from the DNS channel flow code with the previous experimental results by Ergin and White and numerical results by Rizzetta and Visbal. Details of the DNS channel flow code and force field model will be presented in the next section along with mention of key issues in the experimental setup and numerical domain used by Ergin and White and Rizzetta and Visbal, respectively. Results from our DNS channel flow code will be presented and compared to the results obtained by these other groups.

II. Numerical Method and Force Field Model

There exist several approaches to simulating laminar and turbulent boundary layers over textured surfaces. The current investigation uses an immersed boundary method for modeling a variety of surfaces within a spectral DNS code (Goldstein *et al.*[10,11], Goldstein and Tuan[12]). In a spectral method, the spatial distribution of the dependent parameters is commonly modeled with Fourier and Chebychev series in a simple domain. Part of the computation is performed on the parameters themselves and part on the Fourier and Chebychev coefficients of the parameters. Efficient transform methods are used to move between the real and spectral representations. The spectral code used in this work is based on the method in Kim, Moin and Moser[13].

The geometry of interest involves a developing boundary layer in a channel that has a roughness element on the bottom wall. The simulated channel has dimensions of X_L=0.3 m, Y_L=0.0195 m and Z_L=0.019 m, with streamwise flow in the positive x direction. The grid used for this domain consists of over 16 million points, with N_X=1024, N_Y=128 and N_Z=128. Grid points are distributed in the y direction using a cosine grid, such that points are clustered at the top and bottom walls, while a uniform grid is used in the x and z directions. The domain is periodic in the Fourier (spanwise and streamwise) directions; we preserve spanwise periodicity in the computational domain so as to model a spanwise periodic array of roughness elements with a spacing of λ=19 mm. We remove streamwise periodicity from the domain via an absorbing buffer zone (Goldstein *et al.*[14]) which occupies the entire portion of the domain from x=0 to x=0.05 m, as shown in Figure 1. The velocity profile exiting the buffer zone is equivalent to a Blasius profile at x=0.2 m from the flat plate leading edge described by Ergin and White. As the boundary layer profile develops over the length of the domain, the vertical velocity at the boundary layer edge grows as $x^{-1/2}$, which causes a favorable pressure gradient to form in the channel flow. To circumvent this issue, a suction wall

boundary condition was implemented which forces the vertical velocity at the top wall to be equivalent to that of a Blasius solution at each streamwise location, thus allowing for the boundary layer to develop in a zero pressure gradient channel flow. Details of the suction wall are given by Strand[15]. A cylindrical roughness element with diameter d is shown in Figure 1 at x=0.15m. The height of the roughness element is modified in order to examine flow for different Re_k.

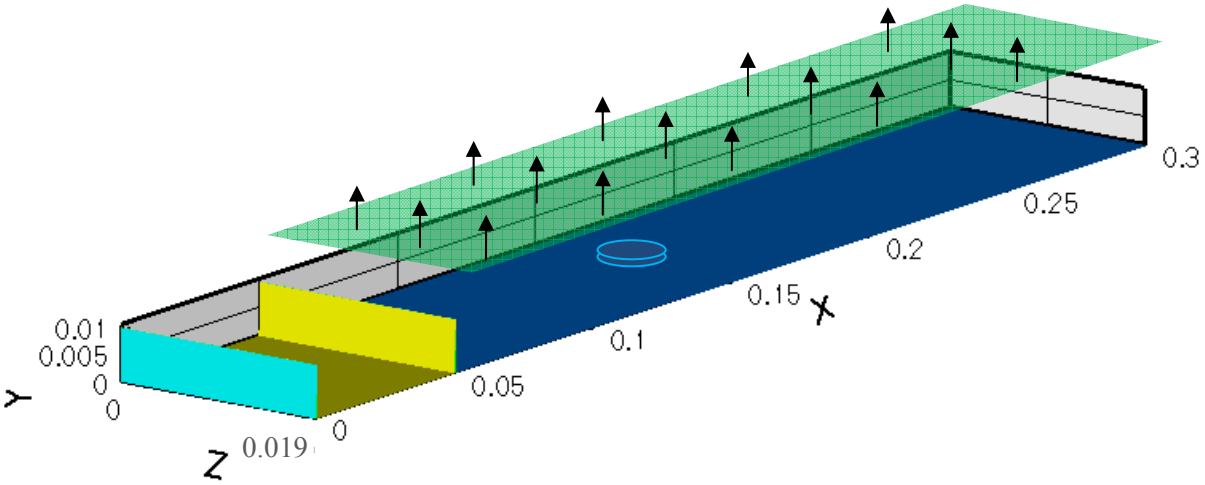

Figure 1. Computational domain used in DNS channel flow. Isosurfaces are shown according to cell type. The buffer region (yellow) is shown on the near side of the domain, beginning at x=0 and ending at x=0.05m. The solid surfaces are shown in dark blue, which include the solid bottom wall and the solid cylindrical roughness element centered at x=0.15m at the spanwise center of the domain. The suction wall is shown in translucent green.

The technique used for modeling the virtual surfaces (cylindrical roughness element, solid wall, buffer zone and suction wall) involves introducing a localized body force field into the Navier Stokes equations. The force field is applied at prescribed locations in the flowfield and dynamically adapts to local flow conditions to bring the flow to a specified velocity thereby creating a virtual surface, which may be either stationary or moving. The applied force is calculated by means of a two-component control scheme which provides feedback based on both the time history of the velocity increment at a prescribed location via the integral term, as well as the current velocity increment at that location:

$$\vec{F}(\vec{x}_s, t) = \alpha \int_0^t \Delta\vec{U}\, dt' + \beta\Delta\vec{U} \qquad (1)$$

The velocity increment at the virtual surface is defined as the difference of the actual and desired velocity:

$$\Delta\vec{U} = \vec{U}(\vec{x}_s, t) - \vec{U}_{des}(\vec{x}_s, t) \qquad (2)$$

This force field technique allows for utilization of the fast transform methods without encountering the severe limitations of a simple geometric domain imposed by most other spectral approaches. To illustrate the effectiveness of the force field method, we examine the flow field near a virtual cylindrical roughness element surface shown in Figures 2(a-d). Contours shown represent instantaneous streamwise velocity in an xy-plane taken at the spanwise center of the domain, and the roughness element is shown outlined in white. Velocity vectors (Figures 2a,b) are shown in white and velocity streamlines (Figures 2c,d) are shown in black. The approaching laminar flow becomes disturbed a couple of cylinder diameters upstream from the actual virtual surface, and several regions of recirculating flow develop just upstream as seen in the streamline patterns shown in Figure 2(c), which are similar to those found in experiments[19] (Figures 2e,f). A larger recirculating flow region forms downstream of the roughness element (Figure 2d). As shown by the velocity vectors near the surface of the roughness element (Figures 2a,b), the force field effectively brings the velocity to zero,

forming a virtual solid surface with a no-slip boundary condition as required. Inside the roughness element, the velocity vectors are negligibly small, but fluctuations in velocity may occur in order to maintain the zero velocity condition at the surface (these fluctuations, however, do not appear to effect the channel flow solution).

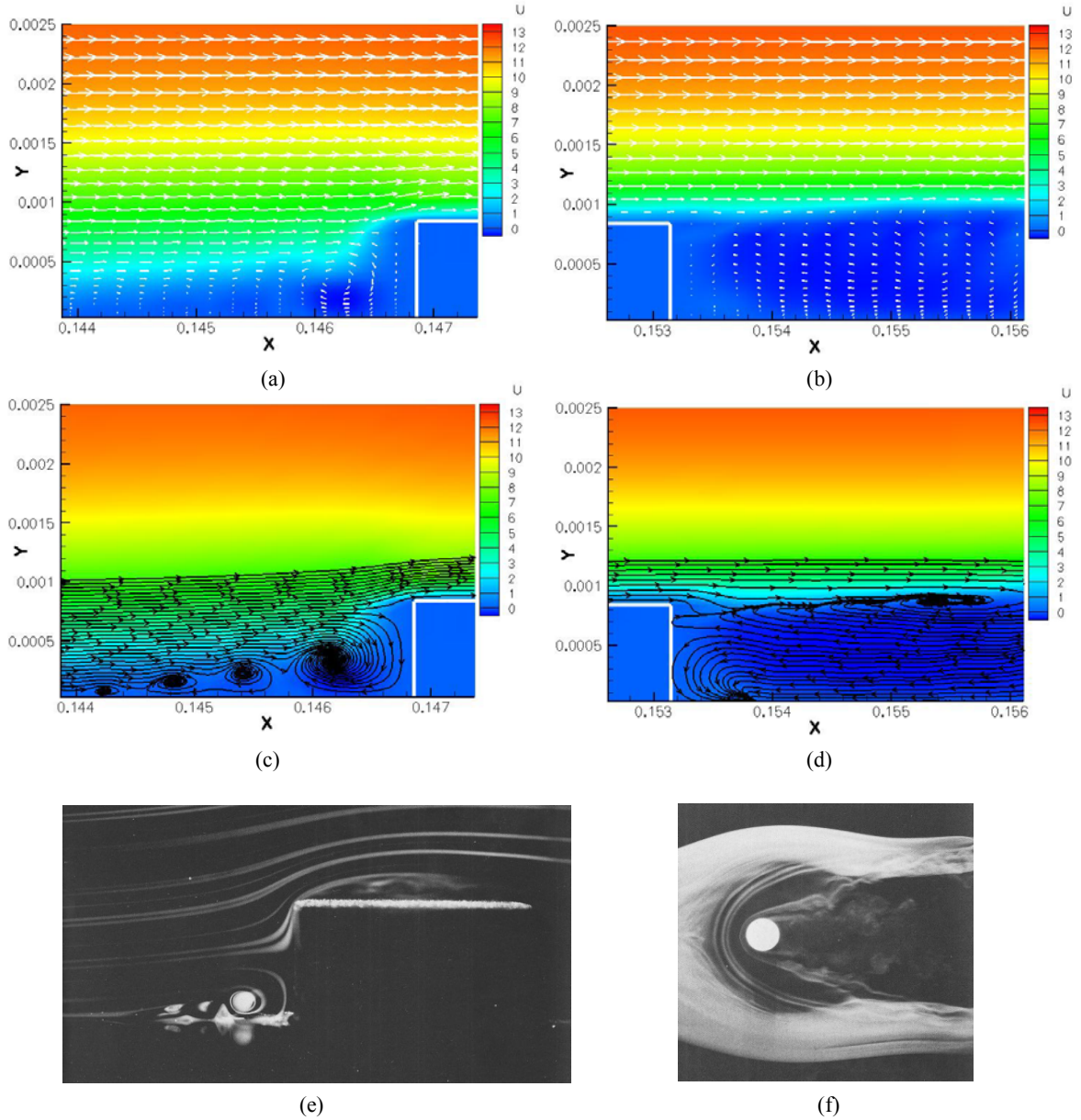

Figure 2. Detailed instantaneous flowfield upstream (a,c) and downstream (b,d) of cylindrical roughness element. Slices are in the xy-plane taken at the spanwise center of the domain and show contours of u (in m/s). The roughness element formed by the force field is outlined in white. Select velocity vectors of (u,v) are shown in white in Fig(a,b) and streamlines are shown in black in Fig(c,d). This particular case corresponds to Re_k=334 or Re_d=5164, with k/δ=0.28. Figures (e,f) show formation of horseshoe vortices ahead of a cylinder (Re_d=5000 in Fig(e), Re_d=4000 in Fig(f), with k/δ≈3 for both) in a laminar boundary layer flow over a flat plate, where visualization is by smoke filaments in air. Images are taken from Van Dyke[16].

The computational domain used by Rizzetta and Visbal was defined (in terms of their nondimensional variables) by -63.5 to 212.5 in x, 0.0 to 5.0 in y, and -9.5 to 9.5 in z. The roughness element was 6.35mm in diameter, was of variable height, and was formed at $(x, y, z) = (0,0,0)$ using

a very fine cylindrical mesh constructed within the surrounding uniform mesh. The solution was spanwise periodic so only one roughness element was modeled in the domain. The experiments conducted by Ergin and White were performed on a flat aluminum plate mounted in an open-return wind tunnel with a freestream of 12.2 m/s. The plate was designed with a 25 mm-long elliptical leading edge and a 300 mm-long trailing edge flap. Roughness elements 6.35 mm in diameter were adhered to the plate 300 mm downstream of the physical leading edge and were spaced 19 mm apart in the spanwise direction. Desired Re_k values were obtained by modifying the roughness heights. Complete details of both setups may be found in either Rizzetta and Visbal[1] or Ergin and White[2].

III. Results for Re_k=202

A. Instantaneous Flowfield

The computational domain is shown in Figure 3(a) in a region close to the roughness element. In the figure, the vortex system generated in front of the cylinder (shown in black as an isosurface of cell type) is highlighted by red streamline rods, and the slices show contours of the magnitude of streamwise vorticity at two positions downstream of the roughness. For this case, only instantaneous flowfield results are presented since time-averaged results are nearly identical. The streamlines shown reveal a system of horseshoe vortices which forms upstream of the cylinder. The primary vortex core forms just upstream of the cylinder approximately 1/8 of a cylinder diameter upstream of the roughness leading edge, and it extends directly downstream. The secondary vortex forms approximately 1/4 of a cylinder diameter upstream of the leading edge of the roughness. The legs of this horseshoe vortex wrap around the cylinder into the downstream region of recirculating flow and then extend downstream. The tertiary vortex core is located approximately 1/3 of a cylinder diameter upstream of the leading edge of the roughness. The legs of the vortex, which gradually lift away from the bottom wall, wrap around the roughness element slightly before extending downstream and decaying. The vortex system exhibits a very gentle initial counter-rotation as the secondary and tertiary vortices intertwine immediately downstream of the cylinder. After approximately one cylinder diameter, there appears to be very little interaction among the vortices, and they decay downstream as indicated by the decrease in the magnitude of streamwise vorticity in the contours.

The flow structures and phenomena seen in our results are different from those obtained by Rizzetta and Visbal, which are shown for comparison in Figure 3(b). Although the x-locations of the contour planes are not specified, it is noted that the streamwise vorticity does show noticeable decay after several roughness diameters in both solutions. However, we see that the number of horseshoe vortices forming upstream of the roughness element is not consistent; the DNS solution obtained by Rizzetta and Visbal captures the primary and secondary vortices described above, but not the tertiary vortex. If we compare the general pattern of the streamtraces originating from the secondary vortex, we see that both DNS solutions show the vortex wrapping around the cylinder and rolling up in the recirculation area of the wake, although the recirculation region appears to extend further downstream in Figure 3(b). The general structure of the primary vortex shows good agreement in both solutions.

We examined the detailed flow about the cylinder in the Re_k=202 case so as to gain a better understanding of the differences observed in our comparison to Rizzetta and Visbal. A brief parametric study was conducted in which we investigated the effects of cylinder shape and grid resolution on our solutions.

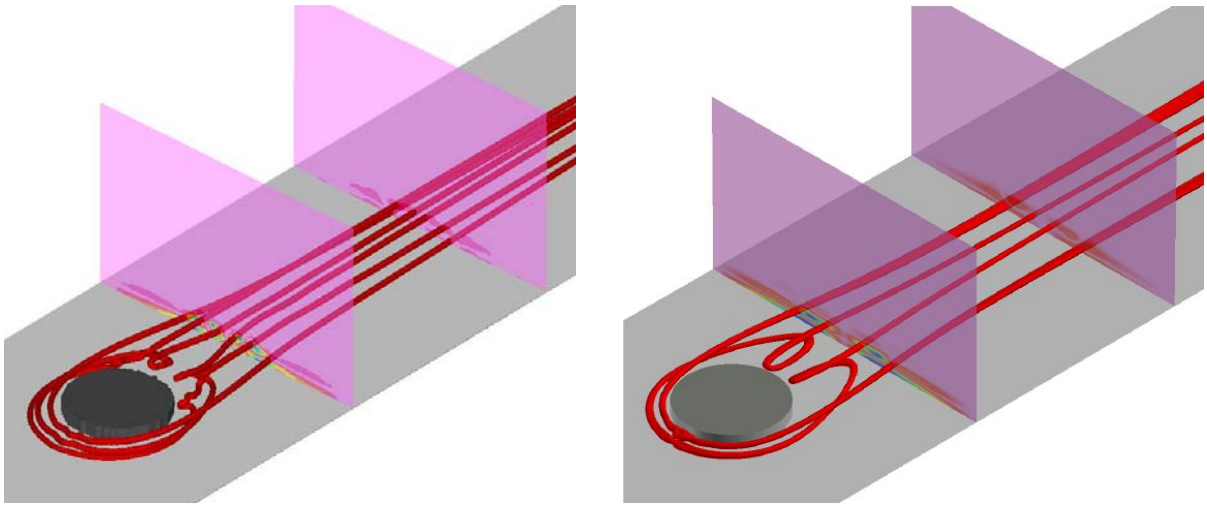

(a) (b)

Figure 3. (a) Instantaneous flowfield for Re_k=202 case. Contour yz-planes show magnitude of streamwise vorticity at x=0.16m and x=0.175m (10mm and 15mm downstream from center of roughness element, respectively). Roughness element is shown as an isosurface, and streamline rods (red) highlight the system of horseshoe vortices formed upstream of the element. (b) Instantaneous flowfield for Re_k=202 case (Rizzetta and Visbal). Contour planes show magnitude of streamwise vorticity, and red streamlines highlight the horseshoe vortex system formed in front of the roughness element.

The shape of the cylinder modeled in this problem is constrained by the grid used in our computational domain. The virtual surface is formed at each point on the cylinder by applying a narrow Gaussian force which is distributed over a prescribed number of the neighboring grid points, so as to create a smoothed virtual surface on a structured grid. The cylinder may be modified by varying either of these two items, so we first consider the particular shape of the surface defined by the grid. The first two shapes examined are identical in height, but the force applied at the grid point defining the leading and trailing edge in Figures 4(a,c) is removed to produce the cylinder shape in Figures 4(b,d). The cylinder (shown in black) is represented as an isosurface of cell type, and the streamribbons and downstream slice show contours of $|\omega|$. In both cases, we see a nearly identical horseshoe vortex system (highlighted by three streamline ribbons) developing just upstream of the roughness in Figures 4(a,b). The regions of high $|\omega|$ shown in the contours of the downstream slice in Figures 4(a,b) are nearly identical despite the modification made to the shape of the leading edge, but the geometry in Figure 4(b) generates slightly less vorticity immediately near the wall at this particular location. If we consider in addition the interaction of the shear layer with the horseshoe vortices, we see from the ribbons (Figures 4(c,d)) that a majority of the vorticity in the wake of the roughness element originates from the shear layer generated over the top of the roughness. The streamline ribbons originating in the shear layer on the right side show a slight initial rotation as the flow passes over the cylinder, and the shear layer becomes slightly modulated in the wake. The ribbons originating from the secondary and tertiary horseshoe vortices become intertwined in the first and second shear layer modules, respectively. We similarly examined various widths of the Gaussian force field used to form a smooth virtual surface, and determined that the effects on the solution were again negligible. Overall, these modifications made to the geometry do not appear to greatly affect the flowfield, so the results presented in this paper are generated by the geometry shown in Figures 4(a,c).

Computations were also obtained on a fine mesh with double the points in the y-direction (N_X=1024, N_Y=256 and N_Z=128) and a coarse mesh with half the points in the z-direction (N_X=1024, N_Y=128 and N_Z=64). In both cases, it was observed that the transition location and the general flow structures were unaffected by the change in wall-normal or spanwise resolution, so the results presented throughout this paper are computed using the mesh mentioned in Section II.

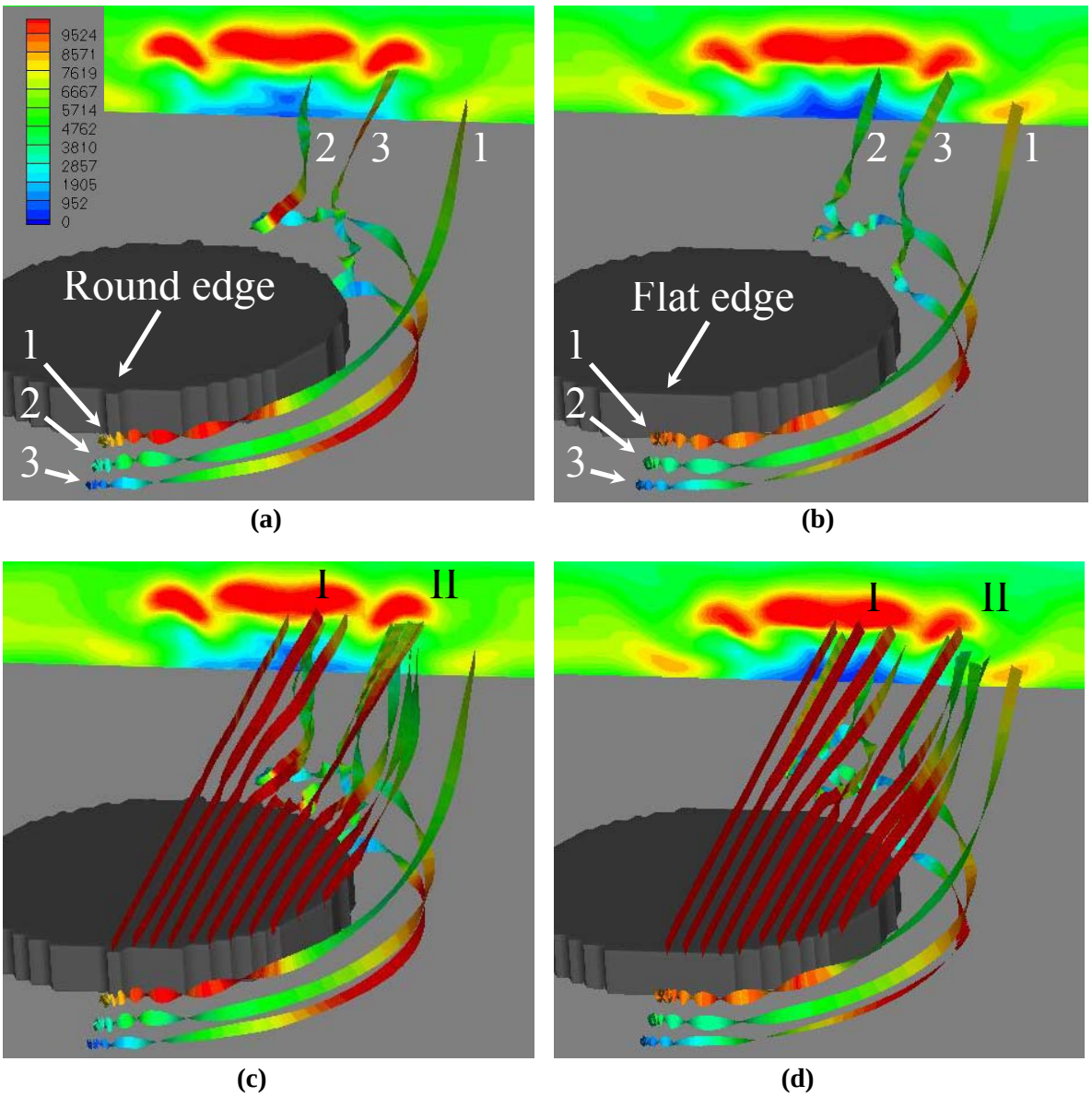

Figure 4. Instantaneous flowfield generated by flow over two different cylinder geometries for the Re_k=202 case. Streamline ribbons and a downstream slice (taken at x=0.16m) show contours of $|\boldsymbol{\omega}|$, and the cylinder is shown as an isosurface of cell type. The primary (1), secondary (2) and tertiary (3) horseshoe vortices are labeled in (a) and (b), and the first (I) and second (II) shear layer modules are labeled in (c) and (d).

Instantaneous streamwise velocity contours taken at several x-locations downstream of the roughness element for Re_k=202 are shown in Figure 5, along with results from Rizzetta and Visbal and Ergin and White. Time-averaged results are not presented for this case since the data are nearly identical. The contours in Figure 5(a-d) show results taken at a distance 10mm downstream of the roughness element. Contours from our numerical studies show additional structure (extra humps) in the near-field wake, a phenomenon which is not observed in the other DNS and experimental solutions at this downstream location. The contours from both Rizzetta and Visbal and Ergin and White show only a single, relatively uniform region of deceleration directly behind the roughness element. In all cases, the flow on either side quickly returns to a largely undisturbed state.

When examining the wake profiles generated by our DNS solution and the experiments, it is important to consider the resolution of both the numerical and experimental grids upon which we are

acquiring and comparing our solutions. The grid used to obtain the DNS solution had a uniform spanwise spacing of 0.1mm and a minimum wall-normal spacing of approximately 0.05mm. The hotwire experiments obtained 0.04mm resolution in the wall-normal direction down to a height 0.47mm above the wall, but measurements below that point could not be obtained due to the limitations of the hotwire data acquisition process. The velocity profile below that point is linearly extrapolated to zero to meet the no-slip condition at the wall. The hotwire was oriented parallel to the wall, so the spanwise resolution was limited to the length of the hotwire, 1.25mm. We applied a filter to our DNS solution so that we could effectively match the wall-normal and spanwise resolution of the experiments, and a linear extrapolation was made below the experimental threshold of 0.47mm. Solutions obtained after applying this filter are shown in the second column of Figure 5. Filtered data in Figure 5b are now in excellent agreement with the experimental results of Figure 5d At distances further downstream of the roughness, the wake from our DNS solution becomes noticeably smoother, and good agreement with the experiments is obtained with or without the filter. In general it is observed that the velocity deficit in the wake persists for at least 10 cylinder diameters downstream, as shown in Figures 5(i-l). The flow for this Re_k in our simulations was not found to be completely steady, however. Small disturbances would develop intermittently a couple of diameters downstream of the roughness, and after convecting 5-8 diameters downstream, generate a region of turbulence near the end of the domain. The solutions presented in Figures (5 -7) were taken during a period in which the flow had re-laminarized.

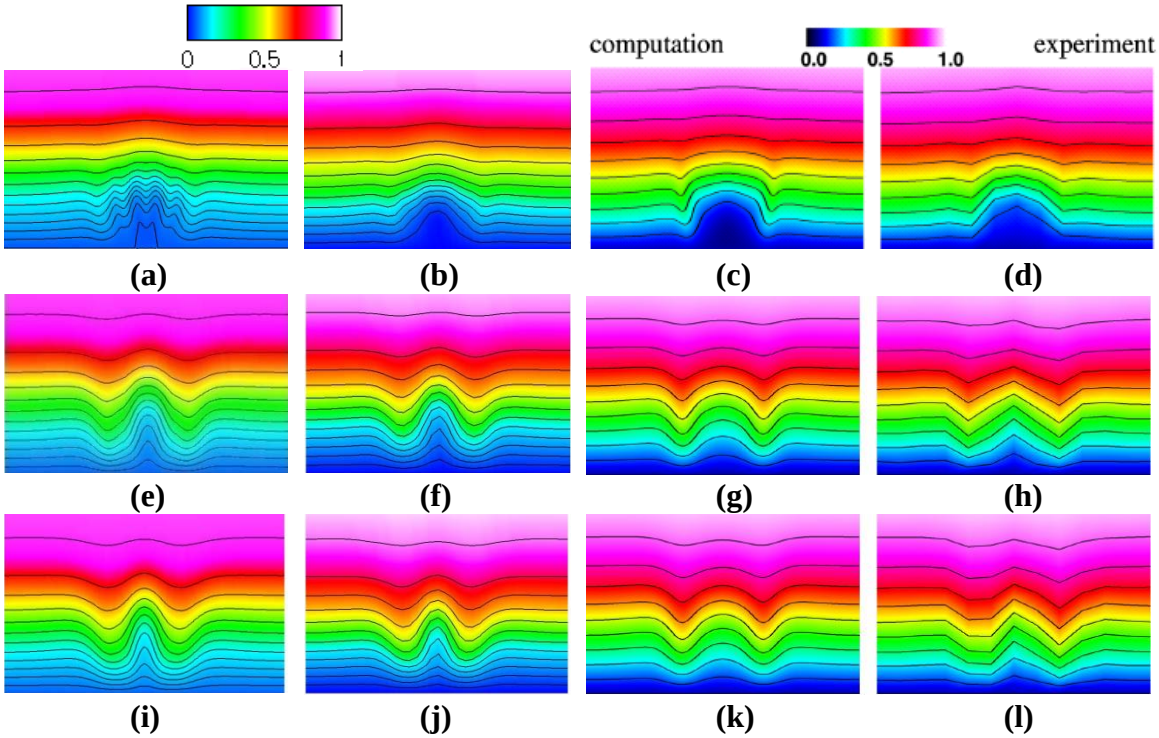

Figure 5. Instantaneous streamwise velocity contours taken at various downstream locations of the cylinder. We compare our unfiltered (first column) and filtered (second column) solutions to those of Rizzetta and Visbal's DNS solutions (third column) and Ergin and White's experimental results (fourth column), all of which show contour slices taken at the same x-locations for Re_k=202. (a-d) Instantaneous streamwise velocity contours taken at x=0.16m (10mm downstream from center of roughness element). (e-h) Instantaneous streamwise velocity contours taken at x=0.19m (40mm downstream of roughness). (i-l) Instantaneous streamwise velocity contours taken at x=0.21m (60mm downstream of roughness). It is noted that the asymmetry seen in the experiment contours (l) is inconsistent with the symmetric DNS contours (i-k) and suggests a flaw in the experimental data.

(a) **(b)**

Figure 6. (a) Instantaneous streamwise velocity contours taken at the spanwise center for Re_k=202 near the roughness element. (b) Comparison of streamwise velocity contours taken at the spanwise center from the current DNS (top) and from Rizzetta and Visbal (bottom).

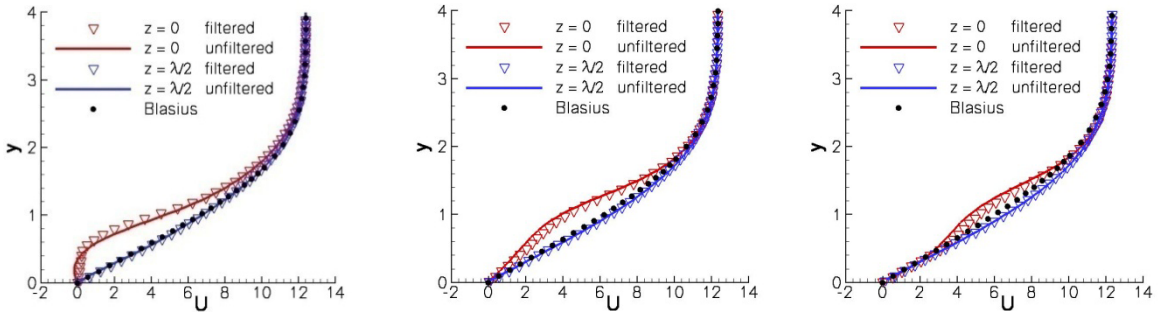

$x = 0.16m$ $x = 0.19m$ $x = 0.21m$

(a) **(b)** **(c)**

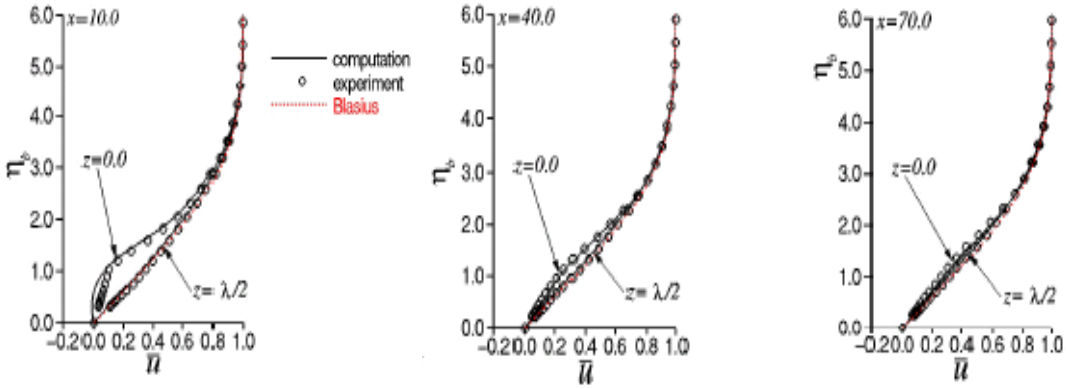

$x = 0.16m$ $x = 0.19m$ $x = 0.22m$

(d) **(e)** **(f)**

Figure 7. Instantaneous streamwise velocity profiles taken at the spanwise center (z=0) and between the roughness elements (z=λ/2) for Re_k=202 at downstream locations of (a) 0.16m, or 10mm downstream of cylinder (b) 0.19m, or 40mm downstream of cylinder and (c) 0.21m, or 60mm downstream of cylinder. Unfiltered results are shown as solid lines, filtered data are shown by open symbols, and the Blasius profile is shown for comparison. These are compared against profiles of time-mean streamwise velocity ($\bar{u}$) obtained by Rizzetta and Visbal at similar downstream locations of (a) 0.16m or 10mm downstream of cylinder (b) 0.19m, or 40mm downstream of cylinder and (c) 0.22m, or 70mm downstream of cylinder. Solid lines represent their DNS solutions, circles show Ergin and White's experimental results, and the Blasius solution is shown in red.

Figure 6 shows the instantaneous streamwise velocity contours on a xy-plane taken at the spanwise center of the domain. In particular, Figure 6(b) shows a comparison of our results for Re_k=202 (top figure) to Rizzetta and Visbal's results (bottom figure), both of which have been stretched in the y-direction by a factor of 3.5. In both cases, we see areas of decelerated flow immediately upstream and downstream of the roughness elements in the recirculation regions. The flow throughout the remainder of the domain exhibits very little disturbance from the roughness and appears to remain smooth.

1-D velocity profiles were taken at the spanwise center and at z=λ/2 downstream of the roughness at several x-locations and are shown in Figure 7(a-c). Here we compare unfiltered (solid line) and filtered (open triangle) profiles to the Blasius solution (filled circle). The first z=0 profile in Figure 7(a) shows a slightly negative streamwise velocity near the wall, due to the recirculating flow region, but the flow between the periodic roughness elements follows the Blasius profile at this location. It is important to note that a hotwire is unable to measure negative velocities and would not be able to capture the reverse flow in the recirculating region. We also observe that the filtered solution does not fully capture the peak negative velocity in the recirculating region due to the linear extrapolation at the wall, and at larger distances from the wall the filtered solution slightly underpredicts the unfiltered streamwise velocity curve. Further downstream in Figures 7(b,c), the flow at z=0 begins to relax toward the Blasius profile, and we see that the profiles at z=λ/2 deviate slightly from the Blasius solution due to spreading of the wake. We also note that the filtered and unfiltered solutions show better agreement near the wall, as the linear extrapolation in the filter becomes more appropriate for these downstream locations, but now the filtered solution slightly overpredicts the unfiltered streamwise velocity further away from the wall.

These profiles are compared against similar profiles presented by Rizzetta and Visbal, in which they have plotted the time-mean streamwise velocity $\bar{u}$ (scaled by the freestream velocity) as a function of η (Figures 7(d-f)). They find a similar recirculating flow region 10mm downstream of the roughness, and the velocity profile begins relaxing towards a Blasius state within 40mm of the cylinder. Their solution indicates, however, that the flow appears to relax more rapidly toward Blasius further downstream of the cylinder as shown in Figure 7(f).

III. Results for Re_k=334

A. Time-averaged Flowfield

Time-averaged streamwise velocity contours taken at several x-locations downstream of the roughness element for Re_k=334 are shown in Figure 8. The contours show unfiltered (first column) and filtered (second column) results in comparison to results obtained by Rizzetta and Visbal (third column). Immediately behind the cylinder at x=0.16m in (a), we observe again a slightly more structured velocity signature in the wake than that observed by Rizzetta and Visbal. This case exhibited rather explosive turbulence downstream of the roughness, and we observe significant mixing in the wake of the cylinder by x=0.19m, as high speed flow begins penetrating the flow region near the wall. If we examine the time-averaged velocity profiles in Figure 9, we see that the flow at the spanwise center of the channel shows initial recirculation in the x=0.16m profile, but takes on a more turbulent boundary layer profile downstream. The wake was highly unsteady and exhibited large amplitude fluctuations which increase with downstream distance. We observed peak fluctuations (normalized by U_∞) of $\mathbf{O}(10^{-1})$ by x=0.19m, which agree quite well with Rizzetta and Visbal's findings, however we observe larger normalized streamwise velocity fluctuations (approximately 0.08, which is nearly 8 times that obtained by Rizzetta and Visbal) closer to the cylinder at x=0.16m. We see in both the streamwise velocity contours in Figure 8 and the velocity profiles in Figure 9 that the turbulent wake had not spread completely across the domain, although we note that the wake spreads significantly more for this case than for the Re_k=202 case.

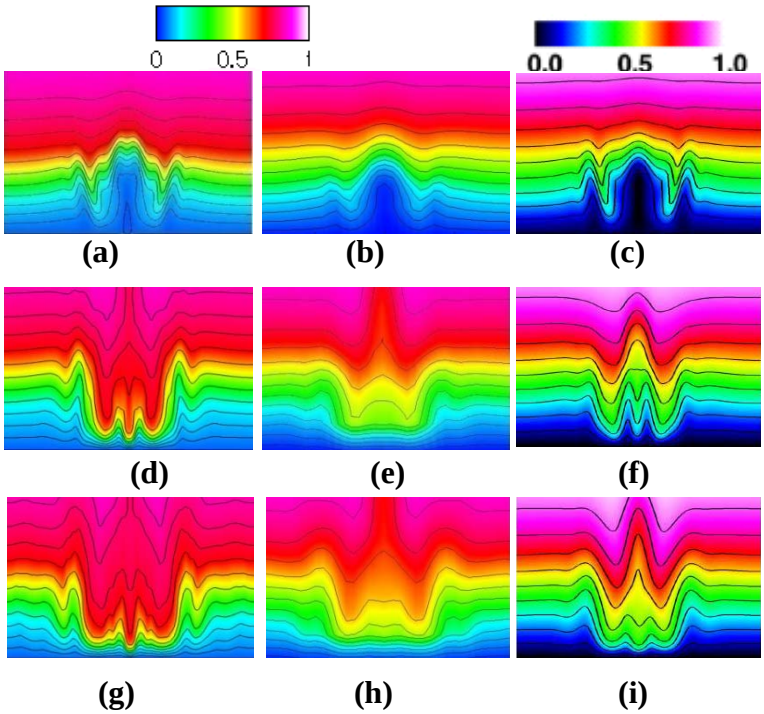

Figure 8. Time-averaged streamwise velocity contours taken at various locations downstream of the cylinder. We compare our unfiltered (first column) and filtered (second column) solutions to those of Rizzetta and Visbal's DNS solutions (third column), all of which show contour slices taken at the same x-locations for Re_k=334. (a-c) Time-averaged streamwise velocity contours taken at x=0.16m (10mm downstream from center of roughness element). (d-f) Time-averaged streamwise velocity contours taken at x=0.19m (40mm downstream of roughness). (g-i) Time-averaged streamwise velocity contours taken at x=0.21m (60mm downstream of roughness). These slices are stretched by a factor of 4 in the y-direction.

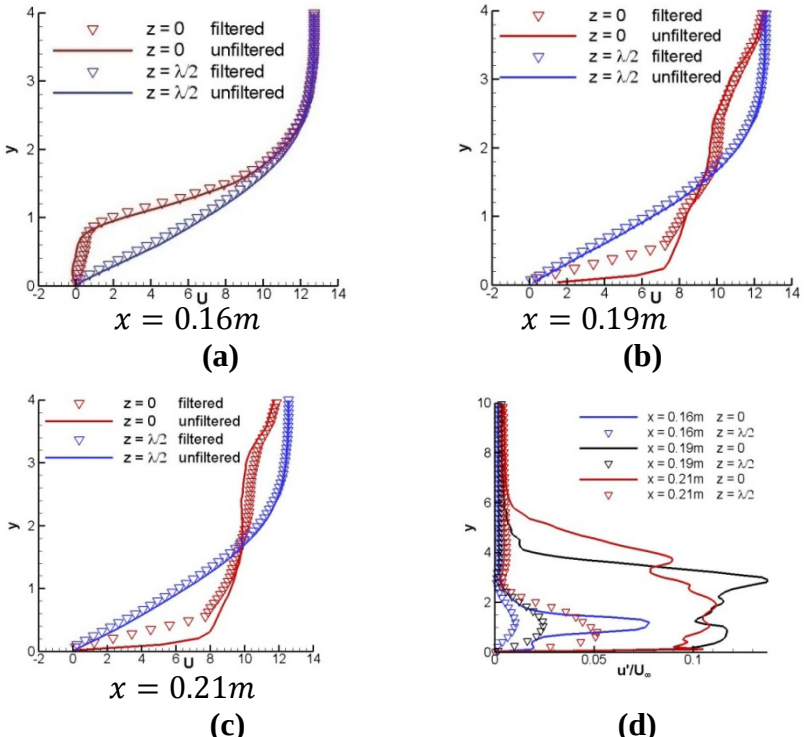

Figure 9. (a-c) Time-averaged streamwise velocity profiles taken at the spanwise center (z=0) and between the roughness elements (z=λ/2) for Re_k=334 at downstream locations of (a) 0.16m, or 10mm downstream of cylinder (b) 0.19m, or 20mm downstream of cylinder and (c) 0.21m, or 60mm downstream of cylinder. Unfiltered results are shown as solid lines and filtered data are shown by open symbols. (d) Profiles of the fluctuating streamwise velocity component u' normalized by the freestream velocity at various spanwise and streamwise locations.

B. Instantaneous Flowfield

Figure 10 shows the instantaneous streamwise velocity contours on an xy-plane taken at the spanwise center of the domain. In particular, Figure 10(b) shows a comparison of our results for (top figure) to Rizzetta and Visbal's results for Re_k=334 (bottom figure), both which have been stretched in the y-direction by a factor of 3.5. In both cases, we observe a rapid transition of the flow several roughness diameters downstream, and the flow remains highly unsteady throughout the remaining length of the domain. Transition appears to occur slightly earlier in the top figure in 10(b), which is consistent with the larger amplitude fluctuations that we observe near the roughness.

The horseshoe vortex system formed in front of the cylinder (shown earlier in Figure 2(c,d)) is characterized by four vortices which extend downstream of the roughness, but they break down rapidly in the wake. If we examine the evolution of the shear layer (highlighted in Figure 11 by contours of $|\omega_z|$) formed off the top of the cylinder, we see that it develops a Kelvin-Helmholtz instability within one cylinder diameter. The shear layer structure appears to roll up and break down within a couple of diameters.

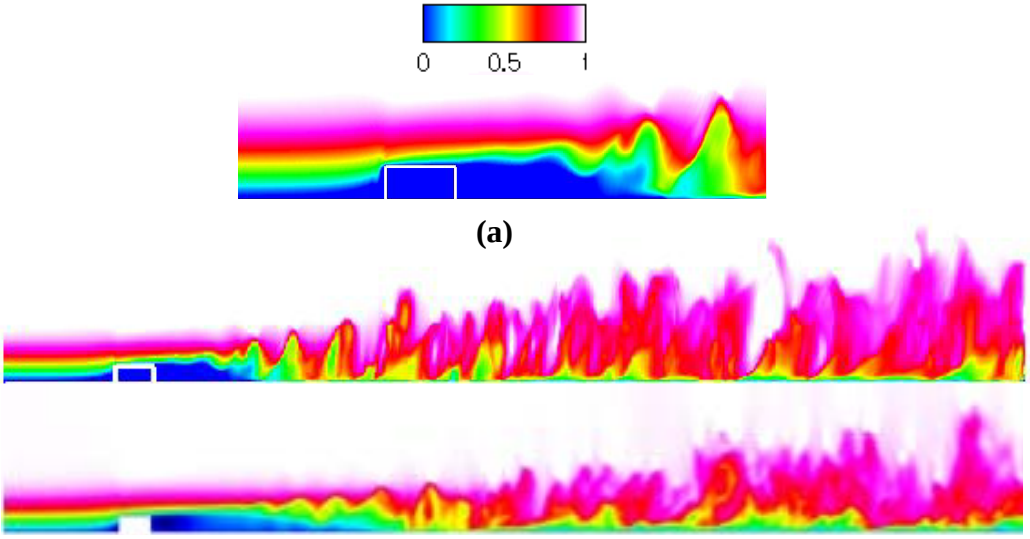

Figure 10. (a) Instantaneous streamwise velocity contours taken at the spanwise center for Re_k=334 near the roughness element. (b) Comparison of streamwise velocity contours taken at the spanwise center for Re_k=334 (top) and for Re_k=334 from Rizzetta and Visbal (bottom).

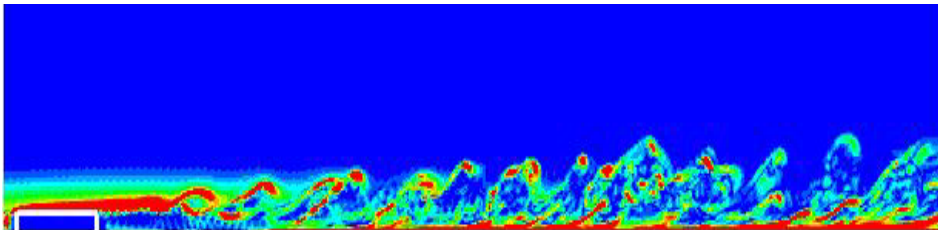

Figure 11. Instantaneous contours of $|\omega_z|$ shown for a xy-slice taken at the spanwise center of the domain for Re_k=334. The cylinder is outlined in white. Weak Gibb's oscillations, characteristic of use of the immersed boundary method in a spectral code, are evident in the flow. Quasi-periodic well-organized structures persist well downstream of the cylinder.

IV. Summary and Conclusions

Direct numerical simulation was used to investigate flow past periodically distributed discrete roughness elements in channel flow. Results were obtained for two different roughness-based Reynolds numbers (Re_k) of 202 and 334. The aim of this paper was to validate the results obtained from our DNS studies against similar numerical investigations by Rizzetta and Visbal and experimental studies by Ergin and White. The flowfield was characterized by a shear layer as well as a system of horseshoe vortices which formed just upstream of the roughness element in both Re_k cases examined. Flowfield visualizations showed that these vortices exhibited streamwise decay for Re_k=202, and in general the flow downstream of the roughness element remained mostly undisturbed throughout the length of the domain with the exception of occasional intermittent bursts of turbulence. Comparison with results from the other groups showed additional structure in the wake near the roughness element, but better comparison to the experimental results was obtained by applying a spatial filter to our DNS solution. This filter allowed us to effectively match the resolution achieved by the hotwire experiments *on the experimental grid*, and the good agreement of our filtered DNS data seems to suggest that the additional structure we see in the near field of the cylinder is a real flow feature. The structure seen in the velocity profiles seems to be largely driven by the modulation that develops in the shear layer over the top of the cylinder. The horseshoe vortex system consisted of three vortices, although only the secondary and tertiary vortices show interaction with the shear layer in the wake.

Reasonable agreement was found between our flowfield results in comparison with Rizzetta and Visbal for the Re_k=334 case. Flowfield visualizations indicated rapid transition behind the roughness element, and the peak amplitude of streamwise velocity fluctuations had reached $\mathbf{O}(10^{-1})$ within 40mm downstream of the roughness in both studies, although we observed relatively larger fluctuations immediately downstream of the cylinder.

Acknowledgements

This work is sponsored by Air Force Office of Scientific Research under grant FA-9550-08-1-0453. The authors would like to also acknowledge the Texas Advanced Computing Center (TACC) for providing the computing resources and technical support for this work.

References

[1] Rizzetta, D.P. and Visbal, M.R., "Direct Numerical Simulations of Flow Past an Array of Distributed Roughness Elements," AIAA Paper 2006-3527, June 2006.
[2] Ergin, F.G. and White, E.B., "Multicomponent and Unsteady Velocity Measurements of Transient Disturbances," AIAA Paper 2005-527, 2005.
[3] Morkovin, M.V., "Bypass Transition to turbulence and research desiderata," *Transition in Turbines*, NASA Conf. Publ. 2386, 1985.
[4] Landahl, M.T., "A note on algebraic instability of inviscid parallel shear flows," *Journal of Fluid Mechanics*, Vol. 98, 1980.
[5] Schmid, P.J. and Henningson, D.S., *Stability and Transition in Shear Flows*, Springer, New York, 2001.
[6] Reshotko, E., "Transient growth: A factor in bypass transition," *Physics of Fluids*, Vol. 13, No. 5, May 2001.
[7] Andersson, P., Berggren, M. and Henningson, D.S., "Optimal disturbances and bypass transition in boundary layers," *Physics of Fluids*, Vol. 11, No. 1, January 1999.

[8] Reshotko, E. and Leventhal, L., "Preliminary experimental study of disturbances in a laminar boundary layerdue to distributed surface roughness," AIAA Paper 81-1224, 1981.
[9] Downs, R.S., White, E.B., Dennisen, N.A., "Transient Growth and Transition Induced by Random Distributed Roughness," *AIAA Journal*, Vol. 46, No. 2, February 2008.
[10] Goldstein, D.B., Handler, R. and Sirovich, L., "Modeling a No-Slip Flow Boundary with an External Force Field," *Journal of Computational Physics*, Vol. 105, pp. 354-366, 1993.
[11] Goldstein, D.B., Handler, R. and Sirovich, L., "Direct Numerical Simulation of Turbulent Flow Over a Modeled Riblet Covered Surface," *Journal of Fluid Mechanics*, Vol. 302, No. 10, pp. 333-376, 1995.
[12] Goldstein, D.B. and Tuan, T.C., "Secondary Flow Induced by Riblets," *Journal of Fluid Mechanics*, Vol. 363, pp. 115-151, 1998.
[13] Kim, J., Moin, P. and Moser, R., "Turbulence Statistics in Fully Developed Channel Flow at Low Reynolds Number," *Journal of Fluid Mechanics*, Vol. 177, pp. 133-166, 1987.
[14] Goldstein, D.B., Cohen, J. and Levinski, V., "DNS of Hairpin Vortex Formation in Poiseuille Flow Due to Two-hole Suction," Presented at 3rd AFOSR Int. Conf. on DNS and LES, Arlington, TX, Aug. 2001.
[15] Strand, J.S., "DNS of Surface Textures to Control the Growth of Turbulent Spots," Masters Thesis, University of Texas at Austin, Austin, TX, 2007.
[16] Van Dyke, M., *An Album of Fluid Motion*, The Parabolic Press, Stanford, CA, 1982.